Middle East Journal of Science

https://dergipark.org.tr/mejs **MEJS**

e-ISSN:2618-6136

Research Article

CHARACTERIZATION OF Cu_2MnSnS_4 THIN FILMS FABRICATED BY SPIN COATING

Canan AYTUĞ AVA*[1, 2] ***Şilan BATURAY***[3]

[1] Dicle University, Science and Technology Application and Research Center, 21280, Diyarbakir, Turkey
[2] Dicle University, Department of Physics, Institute of Natural Sciences, 21280, Diyarbakir, Turkey
[3] Dicle University, Faculty of Science, Department of Physics, 21280, Diyarbakır/Turkey
* Corresponding author; cananaytug@hotmail.com

Abstract*: Cu_2MnSnS_4 (CMTS) thin films are affected by several parameters related to different annealing including sulphur flux rate. In this paper, nontoxic CMTS samples were fabricated onto a soda glass lime substrate by spin-coating to investigate the effect of various sulphur flux rates on the crystal, topological and optical properties by using X-Ray diffraction, scanning electron microscopy, atomic force microscopy, and ultraviolet-visible spectrophotometer, respectively. The X-ray diffraction pattern showed that CMTS films had a main (112) oriented peak and crystallized in a stannite structure. The crystal parameters of CMTS thin films were changed depending on the increase of sulphur flux rate annealed at 550 °C for 90 minutes. The minimum value of dislocation value for CMTS film annealed 30 sccm sulphur flux rate showed the better crystallinity of the film. The scanning electron microscopy images of films showed a decrease in the particle size related to the increased flux of sulphur. AFM images showed that CMTS samples annealed at 40 sccm H2S: Ar had some clumping in the surface topology while CMTS samples annealed at 30 sccm H2S: Ar thin films were uniformly distributed. Ultraviolet-visible spectroscopy (Uv-vis) measurements of the thin films revealed that CMTS film absorbed a high amount of photons as the sulphur flux increased. The energy band gap for the CMTS films was 1.22 and 1.15 eV for 30 sccm and 40 sccm H_2S: Ar, respectively. This work showed that different sulphur flux has a significant effect on the structural and morphological properties of CMTS thin films.*

Keywords*: Sulphur Flux, Thin Film, Optical Properties, Absorbance*

Received: March 30, 2022 *Accepted: June 14, 2022*

1. Introduction

Recently, the requirement for energy is rapidly increasing in both developed and developing countries due to rapid population growth, industrialization, and many other reasons. It is not possible to compensate for this demand with fossil fuels. Therefore, the use of renewable, cheap, and clean energy sources has become compulsory instead of fossil energy resources consumed rapidly and consequently polluting the environment. In recent years, solar cell technologies of nanostructure thin film based on chalcogene thin-film materials, particularly $CuInSe_2$ [1], CuInGa [2], and CdTe [3], are still used in most of the production of photovoltaic devices. Nevertheless, the scarcity of some materials including In and Te in the crust of earth limits the future of solar cells based on CIGS and CdTe, which the extremely expensive [4]. Another problem is that CdTe-based solar cells are a threat to both the environment and health because Cd is a toxic element [5]. Because of these problems, researchers have sought to find more abundant and harmless materials on the earth.

Therefore, direct band gap metal chalcogen thin films have greatly reduced production potential for both raw material and processing requirements in photovoltaic technology. Because Cu_2ZnSnS_4 (CZTS) is one of the most exciting alternatives as an absorber layer in thin-film solar cells [6]. As an alternative to quaternary Cu_2CoSnS_4 (CCTS), $CuInGaS_2$ (CIGS), photovoltaic absorbers have attracted considerable attention in recent years [7]. CMTS is a semiconductor with multiple applications [8,9]. Thus far, solar cells based on Cu_2MnSnS_4 absorbers with conversion efficiencies of up to PCE = 1.8% have been developed [10], which form a tetragonal crystal structure similar to kesterite. It has a direct bandgap at 1.61 eV and a high absorption coefficient [11]. Therefore, it may be resistant to cation disorder, similar to the stannite Cu_2FeSnS_4. Liang et al. describe the synthesis of stannite and wurtzite CMTS nanocrystals via a hot injection approach [12].

CMTS is an excellent p-type semiconducting material that has high absorption coefficient, direct energy band gap varying between 1.1 and 1.3 eV [13-15], and non-toxic and abundant elements in the earth. CMTS solar cells reached an 8.4% yield [16]. Zou et al. found that the nature of the sulfur precursor determines the formation and phase purity of the CZTS material synthesized by the hydrothermal reaction. Furthermore, this phase-control mechanism can be expanded to other quaternary Cu_2MSnS_4 ($M = Cd^{2+}$, Mn^{2+}) nanocrystal syntheses, where the relative reactivity of M^{2+} and the sulfur precursor plays a key role [17].

Shape-controlled topologies have a significant role in the thin film's properties in the nanoscale region. Also, a lot of metals can be employed as doping elements to improve the quality of crystalline thin films' properties with excellent physical and chemical properties of nanostructured thin films. There are various methods to accumulate CMTS absorbers. These methods include electrochemical technique, sol-gel spin coating method, pulsed laser fabrication, thermal evaporation chemical vapor deposition, and magnetron sputtering, [18-23]. The sol-gel spin coating technique has some advantages. Usually, the spin coating is less costly than other methods and requires a simple preliminary preparation. Also, the sol-gel spin coating is one of the best coating methods for obtaining homogeneous and controlled films. For instance, Liu et al. deposited both undoped and 10% Na-doped CZTS thin films using the spin coating technique. They have shown that Na doping can suppress deleterious antisite defects and increase the grain size of CZTS thin films. They also reported improving electrical properties (increase in carrier concentration, mobility, and conductivity due to the NaZn shallow acceptor defect. The study revealed that the power conversion efficiency of the CZTS-based solar cells increased by 44% after Na-doping [24].

Sulphur flux has a large impact on the structural and optical properties of CMTS film. Thus, to get more light on the understanding of the effect of sulphur flux on the physical properties of CMTS films, more experimental studies are necessary. Although there are studies on CMTS films, there is limited information on the effects of sulphur flux on the structural and optical properties of CMTS films using the spin coating technique. Maeda et al. studied the influence of sulfurization temperature on preheated CZTS thin films. They annealed the film between 350 and 600 ◦C for 1 h under a 5% H_2S + N_2 atmosphere. The structural properties of the films indicated that the suitable sulfurization temperature in this work is not lower than 400 ◦C because of the formation of secondary phases including Cu_xS and sulfurization at 560 ◦C is the optimum condition in terms of absorption coefficient [25].

The structure and microstructure of synthetic CMTS depend, among other things, on the nature of these precursors. The development of methods to synthesize CMTS as an absorber in solar cells containing abundant metals that are commonly found on Earth is important to the photovoltaic community due to the similarity of its crystal structure and bandgaps compared with CZTS/CZTSSe, and alongside its increased abundance of Mn compared to Zn [26].

We studied the influence of H_2S: Ar (1:9) flow on the structural, topological, and optical properties of CMTS film. In this study, CMTS samples were formed on glass substrate by using the spin

coating method with different annealing conditions in order to get more information about Cu2MnSnS4 quaternary semiconductor which needed further widespread works on crystal structure, morphological and optical properties. The physical properties of CMTS thin films formed by different sulphur flux rates were investigated according to production conditions. The properties of the obtained thin film were analyzed by X-Ray diffraction (XRD) for crystal structure analysis, scanning electron microscopy (SEM), atomic force microscopy (AFM) for morphological properties, and ultraviolet-visible (UV–vis) spectrophotometry.

2. Experimental

2.1. Preparation of CZTS films

Cu_2MnSnS_4 films at various annealing conditions were deposited on well-cleaned glass substrates by the spin-coated method at a 240 °C substrate temperature. CMTS thin films at two different annealing conditions were deposited by employing a solution containing 0.1 M cupric chloride ($CuCl_2$), 0.1 M manganese chloride ($MnCl_2$), and 0.1 M tin (II) chloride dihydrate ($Cl_2Sn.2H_2O$) as copper, manganese and tin source, respectively. 0.269 g of cupric chloride, 0.252 g of manganese chloride, and 0.451 g of tin (II) chloride dehydrate separately stirred in 20 ml of ethanol, glacial acetic acid (GAA), and a small amount of diethanolamine to regulate pH values for 3 h at 300 K. During the preparation of homogenous solutions, manganese chloride solution was added into cupric chloride solution, and finally, the corresponding amount of tin (II) chloride dihydrate solution was added to manganese chloride/cupric chloride solution. To obtain clear films and remove any residual waste, the SLG substrates were cleaned by boiling in sufficient quantities mixture of H_2O (distilled water), NH_3 (ammonia), and H_2O_2 (hydrogen peroxide) at 105 °C and then in sufficient quantities mixture of H_2O, H_2O_2, and HCl (hydrochloric acid) at 105 °C before fabrication process. Then, each SLG substrate was cleaned in deionized water for 3 min and dried. After obtaining the final solutions and cleaning the substrates, the CMTS films with 2:1:1stoichiometric ratios were spin-coated on substrates at a rate of 5000 rpm for 55 s in air condition. The final solutions were grown onto the substrate by layer and layer and obtained layers were preheated to 240 °C for 10 min in air condition which was seen in Figure1. Having obtained 10 layers of CMTS films, the obtained samples were gradually annealed in the furnace at 30 and 40 sccm H2S: Ar (1:9) flows for 90 minutes at 550 °C, respectively. The sample names were given CMTS (I) and CMTS (II) for 30 sccm and 40 sccm sulphur flux, respectively.

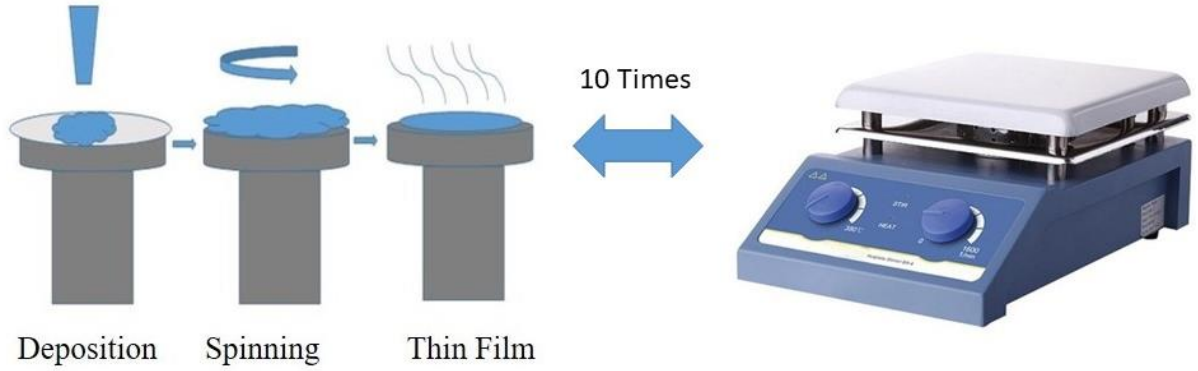

Figure 1. Spin coating processing of thin film

2.2. Characterization

The structural properties including phase identification and crystallographic construction of the obtained films were recorded via X-ray diffractometer patterns with monochromatic Cu Kα radiation using a Bruker D8 Advance diffractometer. The effect of sulphur flux on the CMTS's structural, morphological, and optical properties was investigated in this study. The structural properties including phase identification and crystallographic construction of the obtained films were recorded via X-ray diffractometer patterns with monochromatic Cu Kα radiation using a Bruker D8 Advance diffractometer in the 2θ ranges of 20–60°, step size = 0.02°, step time = 1 s, $\lambda = 1.54187$Å and 40 kV operating voltage as well as the current of 40 mA. The surface morphology of the films was investigated by SEM FEI Quanta 250 FEG scanning electron microscopy and Park System XE-100 atomic force microscopy AFM. The absorbance and the change of optical energy band gap of the obtained samples were recorded with a UV-Vis Spectrophotometer between the wavelength of 1100– 300nm.

3. Results and Discussion

3.1. Structural properties

XRD spectrum played a much more important role in determining the orientation of peaks and crystalline properties of the obtained samples. Figure 2 displays the XRD data of the CMTS film related to sulphur flux rate annealed in a quartz furnace at 550 °C. The XRD patterns of the CMTS(I) sample which exhibited $2\theta \approx 28.23°$ could be indexed to the (112) planes of the stannite CMTS thin film, and the weak diffraction peaks at 46.64° and 47.13° could be indexed to the (220) and (204) planes of CMTS, respectively. As seen in Figure 2, the fact that the XRD patterns of the sample annealed at 40 sccm sulphur flux rate exhibiting a considerable sharpening peak which indicates a strong main peak around $2\theta \approx 28.72°$ could be indexed to the (112) planes of the kesterite Cu_2MnSnS_4 thin film, and the weak diffraction peaks at 47.55°, and 56.40°, could be indexed to the (112), (204), and (312) planes of a single zinc-blende structure, respectively.

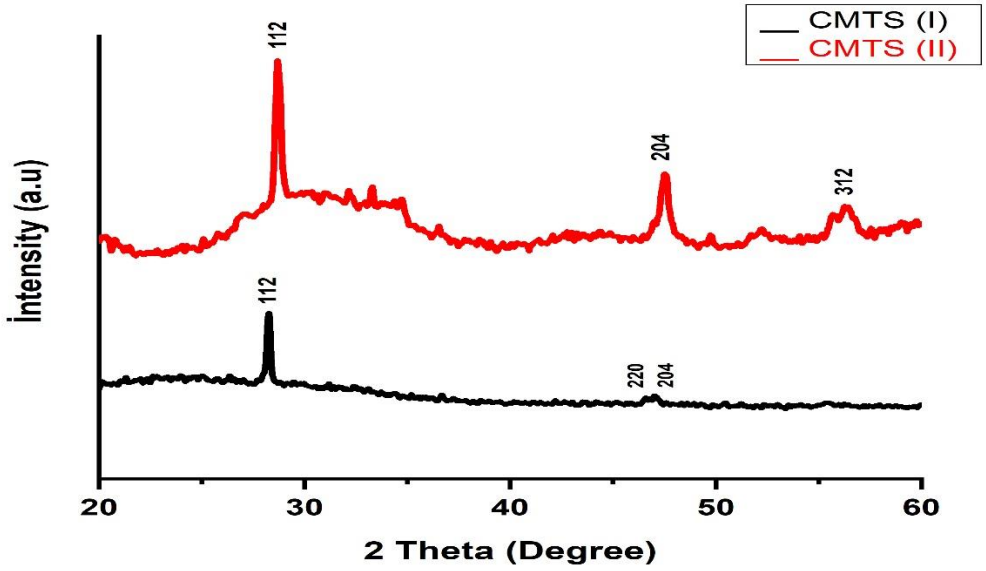

Figure 2. XRD pattern of CMTS thin film

These results showed that the samples crystallized in a single zinc-blende structure owing to the absence of (101), (220), (204), and (312) with the structure of kesterite Cu_2MnSnS_4. Yang et al. [27] indicated that CMTS films obtained by sol-gel method crystallized in a similar structure which was associated with the cations with the random distribution. All these films annealed at 30 and 40 sccm sulphur flux rate showed the main (112) oriented peak. The peak's intensity and full width at half maximum (FWHM) value of the main XRD diffraction peak became sharp and narrower with the increase in the sulphur flux rate, CMTS(I) indicating that (112) orientation had better crystallinity. The calculated interplanar spacing (d), the crystal size (D), the values of strain, and the dislocation density (δ) of all peaks for the CMTS thin films were given in Table 1. As seen in Table 1, the position of main peak 112) planes shifted from 28.23° to 28.72° for the films with increasing H_2S: Ar flow rate. This shift was attributed to the increase of sulphur flux rate effect on the crystal structure of the obtained CMTS samples. As the sulphur flux rate increased from 30 to 40 sccm, a decrease in the FWHM and a change in the intensity of the all CMTS peak obtained by XRD data could be seen in Figure 2. The D value of the CMTS thin film was the smallest (24.45 nm), corresponding to the (204) peak for 40 sccm H_2S: Ar flows. The Scherrer's equation which was used to determine the D value of obtained samples from the XRD data was described as:

$$D = k\lambda/\beta cos\theta \quad (1)$$

where λ was the wavelength of the XRD measurement system (λ = 1.540056 Å), β was the maximum FWHM value of the peaks, θ was the Bragg's angle in degree, and k was the constant which showed shape factor ($k = 0.89$). As seen in Table 1, the D corresponding to the main planes for the sample annealed at 30 sccm (53.2 nm) was higher than the one acquired at 40 sccm sulphur flux rate (28.8 nm). The calculated results displaying the D value of the CMTS films changed with Sulphur flux rate. The largest crystal size value of the main peak showed the good crystalline quality of the sample.

Table 1. Crystal parameters of CMTS thin films grown by spin coating

Sample	2θ(degree)	Calculated d (Å)	FWHM (degree)	Crystal Size (Å)	Strain	Orientation
CMTS (I)	28.23	3.16	0.16	5.32	0.28	112
	46.64	1.95	0.20	4.54	0.20	220
	47.13	1.93	0.24	3.71	0.24	204
CMTS (II)	28.72	3.11	0.30	2.88	0.51	112
	47.55	1.91	0.37	2.45	0.37	204
	56.40	1.63	0.26	3.63	0.21	312

d values of the all CMTS quaternary semiconductor were calculated by the Bragg's equation [28]:

$$2dsin\theta = n\lambda \quad (2)$$

n was a constant which indicated the order of diffraction. The calculated interplanar spacing value of the 40 sccm sulphur flux rate thin films was lower than that of 30 sccm sulphur flux rate thin film (Table 1). n was a constant which indicated the order of diffraction. As seen in Table 1, the calculated interplanar spacing value of the CMTS(II) thin film was lower than that of the CMTS(I) thin film.

The δ value of CMTS film was calculated from the following relation [29]:

$$\delta = \frac{1}{D^2} \quad (3)$$

ε value of all films which is one of the significant factors negatively affecting the crystal structure was calculated by the following equation [30]:

$$\varepsilon = \beta cos\theta/4 \quad (4)$$

The calculated δ values of the main peak for 30 sccm sulphur flux rate changed between 3.54 x 10^{14} m^{-2} and 7.25 x 10^{14} m^{-2}. The calculated δ values of the main peak for 40 sccm sulphur flux rate changed between 7.62 x 10^{14} m^{-2} and 12.09 x 10^{14} m^{-2}. The minimum value of calculated δ obtained for CMTS film annealed 30 sccm sulphur flux showed better crystallinity of the film because calculated δ values were measurement of the amount of defect. As shown in Table 1, dislocation density displayed an increasing tendency from a value of 3.54×10^{14} m^{-2} to a value of 7.25×10^{14} m^{-2} and gave the smallest value of 3.54×10^{14} m^{-2} for the CMTS (I) thin film annealed at 550 °C, corresponding to the maximum value of crystal size. Since the dislocation value was a number of defects in a crystal structure, therefore, the minimum dislocation value obtained in CMTS (I) film approved the good crystallinity of the thin film. Very similarly, the strain value of the CMTS (II) sample for the main peak increased for the samples. Very similarly, the strain value of the annealed at 40 sccm H_2S: Ar flows for the main peak increased for the samples. It was seen from these results that the increase of crystal size for CMTS thin film annealed at 30 sccm H_2S: Ar flows was owing to the decrease in strain value. The ε value was consistent with the enlargement of the d value of main plane. The formation of the defect center could be the induced presence of internal compressive strain [31]. A similar relationship between D and ε and δ was reported. Chen et al. reported that obtained CMTS films were grown by sol-gel technique and annealed with the increase of temperature [32]. It was indicated that while the D increased from 23.41 to 46.82 nm, the strain of the samples decreased from 9.7 × 10−3 to 1.4 × 10−3 and the δ value displayed a decrease from 18×10^{14} to 7×10^{14} lines/m^2 and obtained the lowest value of 4.5×10^{14} lines/m^2 for the samples annealed at 580 °C in the furnace.

3.2. Morphologic analyses

The induced surface changes by varying sulphur flux were studied by SEM, as shown in Figure 3(a-b). According to the SEM images in Figure 3 (a-b), the particle size reduction occurred when the annealing time duration was increased from 30 to 40 sccm sulphur flux rate. It could be suggested that an increase in the flux rate of sulphur could cause a decrease in particle size. Also, when the sulphur flux rate was increased from 30 to 40 sccm, the larger particles could be fragmented into smaller-sized particles. It was said that when the sulphur flux rate was increased, the particle growth deteriorated. The top observation SEM images displayed remarkable modifications with the variation of sulphur flux. Indeed, the film surface of the CMTS(II) sample was covered with randomly spread spherical grains in addition to visible agglomerated grains while the surface morphology of the CMTS(I) film appeared to be more uniform. These changes in surface morphology would have strong effects on optical properties including energy band gap and absorbance. Also, the SEM images of the samples were consistent with the crystal parameters acquired from XRD. In particular, there was a spongy growth containing tiny particles on the thin films [33] and larger particles were shaped on it. Conversely, region-by-region large particle size could occur at the high annealing temperature at high sulphur flux [33, 34]. The results from the study carried out by Olgar et al. of the surface topology of the thin films obtained by the sulphur flux rate at 550 °C annealed temperature utilizing different sulphurization times displayed similar results to our studies [35].

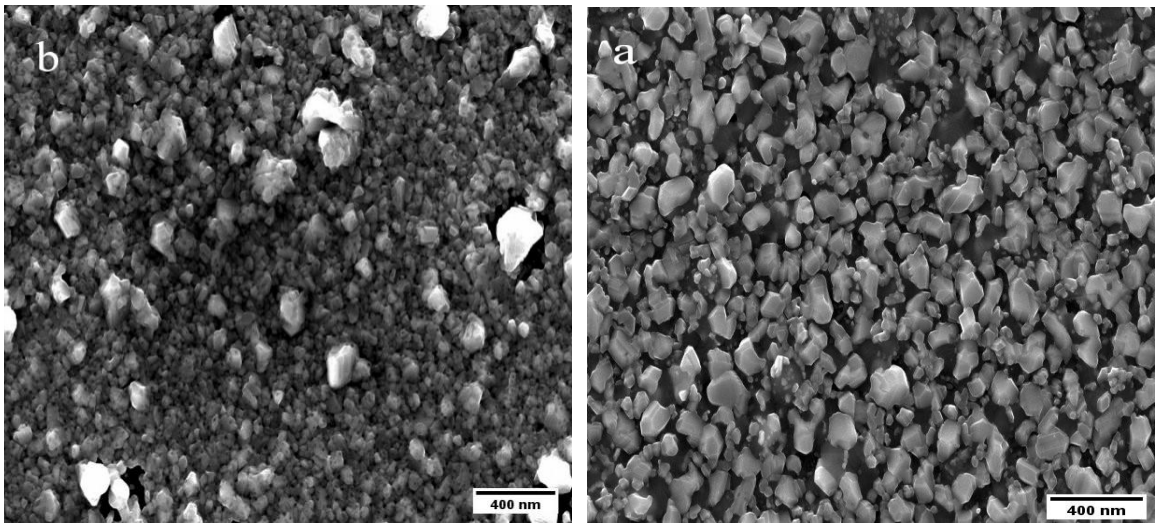

Figure 3 (a-b). a) SEM images of CMTS (I) film, **b)** SEM images of CMTS (II) film

AFM images were obtained using Park System XE-100 to get the correlation between sulphur flux rate and the film topology. All the AFM images morphology was gained by scanning square areas of 12,5 μm × 12,5 μm at a temperature of 273 K. The figures showed the thin films with the structure of grain particles. The 3-D images of AFM of different annealing including sulphur flux rate were given in Figure 4. The figures indicated a 12,5 μm x 12,5 μm area of the thin films with the structure of rod-like and grain particles. The results from obtained AFM images revealed that CMTS thin films were relatively smooth in the valley region while many crystals-like structures were in the hill region which displayed certain orientations. It was seen in AFM image that CMTS(II) sample had some clumping on its surface while the surface morphology of the CMTS(I) film appeared almost uniform. The CMTS film surface was not homogenous. It could be said that AFM images were consistent with the film structure acquired from SEM images.

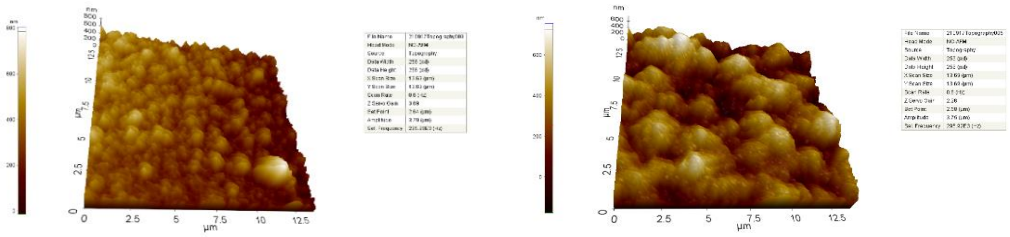

Figure 4. AFM images of CMTS(I) and CMTS(II) thin film, respectively

3.3. Optical properties

Absorbance and energy band gap is one of the most important optical parameters for CMTS thin film. Absorption of the thin films grown on substrates using spin-coating was measured in the range of 1100–300 nm under monochromatic light. The absorption spectrum of the samples implemented by spin coating was shown in Figure 5. It was observed that as the sulphur flux rate of the obtained films increased, they absorbed a high amount of photons. Photon absorption of obtained thin films was reduced in the near-infrared wavelength region.

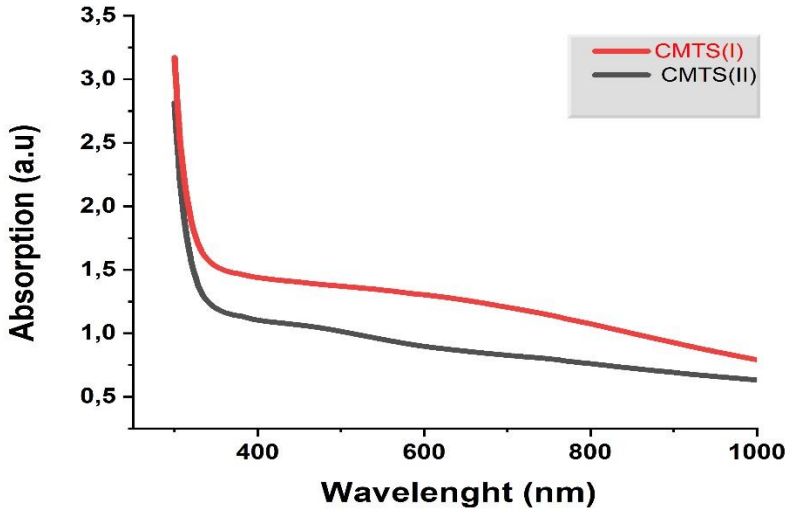

Figure 5. Absorption spectra of thin films

It could be said that the change in absorption values was a result of the different crystal nature of the films and the Moss-Burstein effect [36]. The obtained results showed that the optical properties of CMTS films were modified depending on the sulphur flux rate. The variation in the absorption value of the films indicated that CMTS films could be applied in various optical applications including optical windows and this sample was suitable material for UV filter production.

The band-gap (E_g) of the CMTS samples was calculated using the relation of Tauc [37].

$$\alpha h\upsilon = A\left(h\upsilon - E_g\right)^2 \tag{5}$$

where A is a constant, $h\upsilon$ is photon energy and the value of n was taken to be $1 / 2$. Figure 6. showed the plot of the optical energy band gap which was calculated by a straight line of $(\alpha h\upsilon)^2$ (versus $(h\upsilon)$) in Tauc plot. As seen in the figure, the energy band gap was found as 1.22 and 1.15 eV for CMTS(I) and CMTS(II) thin film, respectively. According to XRD and SEM results, the crystal size decreased and the density of grain increased with the increase of H_2S: Ar (1:9) flows. Thus, the possibility of the scattering of the electron at grain boundaries decreases, and electronic shift from the valence band to the conduction band occurs more easily, which outcomes in the decreasing of energy band gap value.

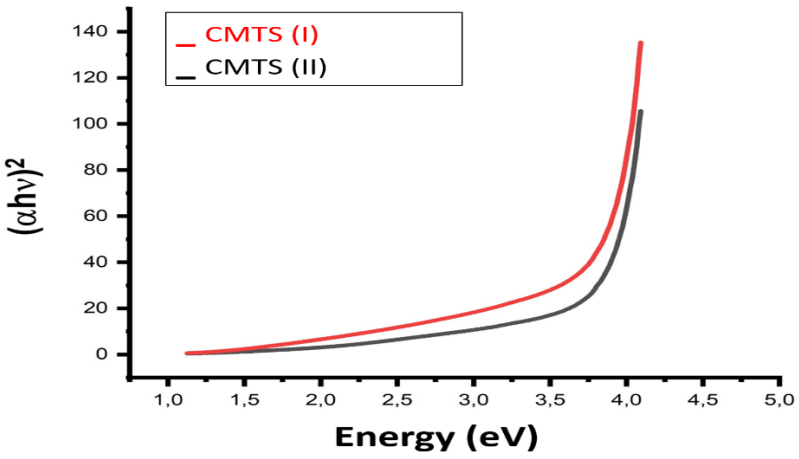

Figure 6. The energy band gap of thin films

The seen change in E_g value might be because of the difference in the crystallinity nature of the film. The decreasing of energy band gap values was owing to the effect of the change of crystalline quality in obtained films. Chen et al indicated that the (E_g) values of CMTS quaternary semiconductor films were changed between 1.62–1.14 eV related to the temperature of post-annealing [32]. Yu et al. [38] reported that the energy band gap decreased related to the rise of the Cu/(Mn + Sn) ratio which improved the photovoltaic performance. Paier et al. reported that the energy band gap of films changed to higher energies as Cu/(Zn+Sn) decreased [39]. This change was due to the fact that the valance band of films was composed of a linear combination with antibonding between Cu 3d orbital and S 3p orbitals. Optical properties of samples were detected using conversion from Cu 3d/S 3p levels into conduction band; this could be attributed to changes in the band gap.

4. Conclusion

In summary, CMTS films were grown on a substrate of soda-lime glass by a spin coating method and annealed at 550 °C for 90 minutes in the furnace depending on the sulphur flux. The effect of sulphur flux on the structural, morphological, and optical properties of the film was investigated. It was observed that the CMTS(I) thin-film had (112) oriented main peaks with good crystallinity and low strain value. The XRD parameters including crystal size, dislocation density, and microstrain values were changed with increasing the H_2S: Ar flow. The smallest value 3.54×10^{14} m^{-2} for the CMTS(I) thin film was annealed at 550 °C, corresponding to the maximum value of crystal size. The crystallinity of the CMTS thin film was considerably improved at 30 sccm H_2S: Ar flow. SEM images revealed that the larger particles could be fragmented into smaller-sized particles. AFM images revealed that CMTS thin films were relatively smooth in the valley region while many crystals-like structures were seen in the hill region. It was observed that the films absorbed a higher amount of photons as the sulphur flux increased and there is a decrease in the infrared region. E_g values of the films were calculated as 1.22 and 1.15 eV for CMTS(I) and CMTS(II), respectively. It is said that the H_2S: Ar flow was effective on the energy band gap and the crystalline quality in obtained films. As a result, CMTS(I) with optimal properties was determined to be used as an absorber layer in a solar cell and the variation in the absorption value of the films indicated that CMTS(I) flux could be also applied in various optical applications including optical windows and UV filter production. In this study, we experimentally showed that the cationic

substitution of Zn by Mn could change the physical properties including absorbance and energy band gap of CZTS material.

Acknowledgments

We thank Dicle University Science and Technology Application and Research Center (DUBTAM) for their support of our study.

Ethical Statements

The author declares that this study does not require ethics committee approval or any special permission and does not cause any harm to the environment.

Conflict of interest

The authors declare no conflict of interest.

Authors Contributions

CAA ve SB carried out the experiments and wrote the manuscript. The authors discussed the results and contributed to the final article.

References

[1] A. Rockett, R. Birkmire, $CuInSe_2$ for photovoltaic applications, *Journal of Applied Physics* 70(7) R81-R97, 1991.

[2] C.-Y. Su, W.-H. Ho, H.-C. Lin, C.-Y. Nieh, S.-C. Liang, The effects of the morphology on the CIGS thin films prepared by CuInGa single precursor, *Solar energy materials and solar cells* 95(1) 261-263, 2011.

[3] J. Britt, C. Ferekides, Thin-film CdS/CdTe solar cell with 15.8% efficiency, *Applied physics* letters 62(22), 2851-2852, 1993.

[4] S. Kahraman, S. Çetinkaya, M. Podlogar, S. Bernik, H. Çetinkara, H. Güder, Effects of the sulphurization temperature on sol gel-processed Cu_2ZnSnS_4 thin films, *Ceramics International* 39(8), 9285-9292, 2013.

[5] X. Wu, High-efficiency polycrystalline CdTe thin-film solar cells, *Solar Energy* 77(6) 803-814, 2004.

[6] J. K. Larsen, F. Larsson, T. Törndahl, N. Saini, L. Riekehr, Y. Ren, C. Platzer- Björkman, Cadmium free Cu_2ZnSnS_4 solar cells with 9.7% efficiency, *Advanced Energy Materials* 9(21), 1900439, 2019.

[7] J.-S. Seol, S.-Y. Lee, J.-C. Lee, H.-D. Nam, K.-H. Kim, Electrical and optical properties of Cu_2ZnSnS_4 thin films prepared by rf magnetron sputtering process, *Solar energy materials and solar cells* 75(1-2), 155-162, 2003.

[8] H. Guan, X. Wang, Y. Huang, Optical, photocatalytic and thermoelectric properties of Cu_2MeSnS_4 (Me= Mn 2, Fe 2, Co 2) nanocrystals via microwave-assisted solvothermal method, *Chalcogenide Letters* 15(9), 435-440, 2018.

[9] H. Guan, H. Hou, M. Li, J. Cui, Photocatalytic and thermoelectric properties of Cu_2MnSnS_4 nanoparticles synthesized via solvothermal method, *Materials Letters* 188, 319-322, 2017.

[10] X. Li, Z. Hou, S. Gao, Y. Zeng, J. Ao, Z. Zhou, Y. Zhang, B. Da, W. Liu, Y. Sun, Y. Zhang, Efficient optimization of the performance of Mn^{2+}-doped kesterite solar cell: Machine learning aided synthesis of high efficient $Cu_2(Mn, Zn)Sn(S, Se)_4$ Solar Cells, *Solar RRL* 2(12), 1800198, 2018.

[11] J. Yu, H. Deng, Q. Zhang, J. Tao, L. Sun, P. Yang, J. Chu, The role of sulfurization temperature on the morphological, structural and optical properties of electroplated Cu_2MnSnS_4 absorbers for photovoltaics, *Materials Letters* 233, 111-114, 2018.

[12] K. Rudisch, W.F. Espinosa- García, J.M. Osorio- Guillén, C.M. Araujo, C. Platzer- Björkman, J.J. Scragg, Structural and electronic properties of Cu_2MnSnS_4 from experiment and First-Principles calculations, *Physica status solidi (b)* 256(7), 1800743, 2019.

[13] X. Liang, P. Guo, G. Wang, R. Deng, D. Pan, X. Wei, Dilute magnetic semiconductor Cu_2MnSnS_4 nanocrystals with a novel zincblende and wurtzite structure, *RSC Advances* 2(12), 5044-5046, 2012.

[14] Y. Cui, R. Deng, G. Wang, D. Pan, A general strategy for synthesis of quaternary semiconductor Cu_2MSnS_4 (M= Co^{2+}, $Fe^{2+,}$ Ni^{2+}, Mn^{2+}) nanocrystals, *Journal of Materials Chemistry* 22(43), 23136-23140, 2012

[15] M. Quintero, E. Moreno, S. Alvarez, J. Marquina, C. Rincón, E. Quintero, P. Grima, J.-A. Heano, M.A. Macías, Lattice parameter values and phase transitions for the Cu_2-II-IV-S_4 (Se_4)(II= Mn, Fe, Co; IV= Si, Ge, Sn) magnetic semiconductor compounds, Rev. *LatinAm. Metal. Mater.* 34(1), 2014.

[16] T.K. Todorov, K.B. Reuter, D.B. Mitzi, High-efficiency solar cell with earth-abundant liquid-processed absorber, *Advanced Materials* 22(20), 156-159, 2010.

[17] Y. Zou, X. Su, J. Jiang, Phase-controlled synthesis of Cu_2ZnSnS_4 nanocrystals: the role of reactivity between Zn and S, *Journal of the American Chemical Society* 135(49), 18377-18384, 2013.

[18] P.K. Sarswat, M. Snure, M.L. Free, A. Tiwari, CZTS thin films on transparent conducting electrodes by electrochemical technique, *Thin Solid Films* 520(6), 1694-1697, 2012.

[19] K. Tanaka, N. Moritake, H. Uchiki, Preparation of Cu_2ZnSnS_4 thin films by sulphurizing sol–gel deposited precursors, *Solar energy materials and solar cells* 91(13), 1199-1201, 2007.

[20] S. Vanalakar, G. Agawane, S. Shin, M. Suryawanshi, K. Gurav, K. Jeon, P. Patil, C. Jeong, J. Kim, J. Kim, A review on pulsed laser deposited CZTS thin films for solar cell applications, *Journal of Alloys and Compounds* 619, 109-121, 2015.

[21] Y. Lu, S. Wang, Z. Li, Z. Jiang, M. Yang, Q. Li, Effects of sputtering period on the performance of Cu_2ZnSnS_4 solar cells, Physica B: Condensed Matter 507, 35-40, 2017.

[22] A. Tombak, Y.S. Ocak, M.F. Genişel, T. Kilicoglu, Electrical and optical properties of Cu_2ZnSnS_4 grown by a thermal co-evaporation method and its diode application, *Materials Science in Semiconductor Processing* 28, 98-102, 2014.

[23] M.Z. Ansari, N. Khare, Structural and optical properties of CZTS thin films deposited by ultrasonically assisted chemical vapour deposition, *Journal of Physics D: Applied Physics* 47(18), 185101, 2014.

[24] B. Liu, J. Guo, R. Hao, L. Wang, K. Gu, S. Sun, A. Aierken, Effect of Na doping on the performance and the band alignment of CZTS/CdS thin film solar cell, *Solar Energy* 201, 219-226, 2020.

[25] K. Maeda, K. Tanaka, Y. Nakano, H. Uchiki, Annealing temperature dependence of properties of Cu_2ZnSnS_4 thin films prepared by sol-gel sulfurization method. *Japanese Journal of Applied Physics* 50(5S2), 05FB08, 2011.

[26] E. Waluś, M. Manecki, G. Cios, T. Tokarski, Effect of a sulfur precursor on the hydrothermal synthesis of Cu_2MnSnS_4, *Materials* 14(13), 3457, 2021.

[27] G. Yang, X. Zhai, Y. Li, B. Yao, Z. Ding, R. Deng, H. Zhao, L. Zhang, Z. Zhang, Synthesis and characterizations of Cu_2MgSnS_4 thin films with different sulphuration temperatures, *Materials Letters* 242, 58-61, 2019.

[28] J. Shaikh, R.C. Pawar, R.S. Devan, Y.-R. Ma, P.P. Salvi, S.S. Kolekar, P.S. Patil, Synthesis and characterization of Ru doped CuO thin films for supercapacitor based on Bronsted acidic ionic liquid, *Electrochimica Acta* 56(5), 2127-2134, 2011.

[29] V.T. Tiong, Y. Zhang, J. Bell, H. Wang, Phase-selective hydrothermal synthesis of Cu 2 ZnSnS 4 nanocrystals: the effect of the sulphur precursor, *CrystEngComm* 16(20), 4306-4313, 2014.

[30] M. Saleem, L. Fang, A. Wakeel, M. Rashad, C. Kong, Simple preparation and characterization of nano-crystalline zinc oxide thin films by sol-gel method on glass substrate, 2012.

[31] J.J. Scragg, T. Ericson, X. Fontané, V. Izquierdo-Roca, A. Pérez-Rodríguez, T. Kubart, M. Edoff, C. Platzer-Björkman, Rapid annealing of reactively sputtered precursors for Cu_2ZnSnS_4 solar cells, Progress in Photovoltaics: *Research and Applications* 22(1), 10-17, 2014.

[32] L. Chen, H. Deng, J. Tao, W. Zhou, L. Sun, F. Yue, P. Yang, J. Chu, Influence of annealing temperature on structural and optical properties of Cu_2MnSnS_4 thin films fabricated by sol-gel technique, *Journal of Alloys and Compounds* 640, 23-28, 2015.

[33] J. Jiang, L. Zhang, W. Wang, R. Hong, The role of sulphur in the sulphurization of CZTS layer prepared by DC magnetron sputtering from a single quaternary ceramic target, *Ceramics International* 44(10), 11597-11602, 2018.

[34] W. Wang, G. Wang, G. Chen, S. Chen, Z. Huang, The effect of sulphur vapor pressure on Cu_2ZnSnS_4 thin film growth for solar cells, *Solar Energy* 148 12-16, 2017.

[35] M. Olgar, A. Seyhan, A. Sarp, R. Zan, Impact of sulphurization parameters on properties of CZTS thin films grown using quaternary target, *Journal of Materials Science*: Materials in Electronics 31(22), 20620-20631, 2020.

[36] S. Manjunatha, R.H. Krishna, T. Thomas, B. Panigrahi, M. Dharmaprakash, Moss-Burstein effect in stable, cubic ZrO_2: Eu^{+3} nanophosphors derived from rapid microwave-assisted solution-combustion technique, *Materials Research Bulletin* 98, 139-147, 2018.

[37] J. Tauc, Amorphous and liquid semiconductors, Springer Science & Business Media, 2012.

[38] J. Yu, H. Deng, Q. Zhang, J. Tao, L. Sun, P. Yang, J. Chu, The role of sulphurization temperature on the morphological, structural and optical properties of electroplated Cu2MnSnS4 absorbers for photovoltaics, *Materials Letters* 233, 111-114, 2018.

[39] J. Paier, R. Asahi, A. Nagoya, G. Kresse, Cu_2ZnSnS_4 as a potential photovoltaic material: a hybrid Hartree-Fock density functional theory study, *Physical Review B* 79(11), 115126, 2009.